Thin-Film Thermal Conductivity Measurement Using Microelectrothermal Test Structures and Finite-Element-Model-Based Data Analysis

Nenad Stojanovic, Jongsin Yun, Erika B. K. Washington, Jordan M. Berg, *Senior Member, IEEE*, *Member, ASME*, Mark W. Holtz, and Henryk Temkin, *Fellow, IEEE*

***Abstract*—We present a new method for measuring thermal conductivities of films with nanoscale thickness. The method combines a microelectrothermal test structure with a finite-element-based data analysis procedure. The test device consists of two serpentine nickel structures, which serve as resistive heaters and resistance temperature detectors, on top of the sample. The sample is supported by a silicon nitride membrane. Analytical solution of the heat flow is infeasible, making interpretation of the data difficult. To address this, we use a finite-element model of the test structure and apply nonlinear least-squares estimation to extract the desired material parameter values. The approach permits simultaneous extraction of multiple parameters. We demonstrate our technique by simultaneously obtaining the thermal conductivity of a 280 μm$\times$ 80 μm$\times$ 140 nm thick aluminum sample and the 360 μm$\times$ 160 μm$\times$ 180 nm thick silicon nitride support membrane. The thermal conductivity measured for the silicon nitride thin film is 2.1 W/mK, which is in agreement with reported values for films of this thickness. The thermal conductivity of the Al thin film is found to be 94 W/mK, which is significantly lower than reported bulk values and consistent both with reported trends for thin metallic films and with values that were obtained using electrical resistivity measurements and the Wiedemann–Franz law. [2007-0033]**

***Index Terms*—Measurement, microthermal devices, thermal conductivity, thermal variables measurement, thin films.**

I. Introduction

THE THERMAL conductivities of films with submicrometer thickness are known to differ significantly from those of bulk samples of the same material [1]–[3]. This difference is increasingly important, as electronic devices—in microelectronics, microelectromechanical systems, and optoelectronics—shrink in size and thermal management becomes a limiting factor in performance [4]–[7]. As devices are developed at the nanoscale range, the need for a better understanding of fundamental material properties is becoming more acute. This paper presents a novel technique for the measurement of these properties—well suited to small structures—that combines microfabricated electrothermal test devices with a model-based data processing approach using finite-element analysis (FEA). This technique relaxes design constraints on the material sample geometry, facilitating fabrication.

There are many approaches to the measurement of thin-film thermal properties [8]–[20]. Thermoreflectance may be used for noncontact characterization of thin-film thermal conductivity [9], [20]. In the 3ω method, an alternating current is applied to the heater/sample/sensor structure, and a lock-in amplifier is used to detect the current or voltage output signal at a particular frequency [1], [11], [14]. Another well-known method is based on steady-state joule heating with dc current excitation [9]. For thermometric methods, in which heat is made to flow through a sample and the resulting temperature changes detected, interpretation of the results is simplified if heat transfer is primarily through the sample and can be modeled using straightforward analytical approaches. To ensure that sufficient heat passes through the sample for an adequate study of its properties, any supporting structures should have a thermal resistance that is at least comparable to, and preferably much higher than, that of the sample. Therefore, when extending this approach to thin films, the sample may be supported on a structural membrane, or window, of submicrometer thickness. Fabrication limitations lead to test structures that are only slightly smaller than the windows themselves; hence, the potential for parasitic heat loss through the associated support, power, and sensing structures is significant.

To address these issues, some researchers adjust the sample geometry [13], whereas others create sophisticated and delicate suspended structures [8]. Furthermore, in [8], a series of measurements is made on partially fabricated structures to isolate the effect of each layer. Another possibility, which has not been fully explored, is to relax the need for analytical solution of the heat transfer by using FEA models. FEA has been shown to be a reliable tool for analysis of microfabricated thermal measurement systems [21], [22]. For example, La Spina *et al.* use FEA to characterize the geometry of heat flow through their device [13]. However, FEA

Manuscript received February 9, 2007; revised April 16, 2007. This work was supported in part by the National Science Foundation under Grant CTS-0210141 and in part by the J. F. Maddox Foundation. Subject Editor E. Obermeier.

N. Stojanovic and M. W. Holtz are with the Department of Physics and the Nano Tech Center, Texas Tech University, Lubbock, TX 79409 USA.

J. Yun is with the System LSI Technology Development Group, Samsung Semiconductor, Seoul 143-224, Korea.

E. B. K. Washington is with the Department of Mechanical Engineering, University of Alberta, Edmonton, AB T6G 2G8 Canada.

J. M. Berg is with the Department of Mechanical Engineering and the Nano Tech Center, Texas Tech University, Lubbock, TX 79409 USA (e-mail: jordan.berg@ttu.edu).

H. Temkin is with the Department of Electrical and Computer Engineering and the Nano Tech Center, Texas Tech University, Lubbock, TX 79409 USA.

Color versions of one or more of the figures in this paper are available online at http://ieeexplore.ieee.org.

Digital Object Identifier 10.1109/JMEMS.2007.900877

1057-7157/$25.00 © 2007 IEEE

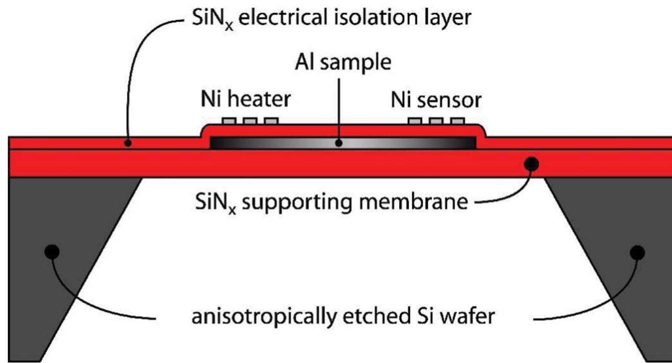

Fig. 1. Schematic cross section of the test structure (not to scale). One layer of silicon nitride supports the sample for fabrication, and the second layer electrically insulates the sample from the heater/sensors. This schematic shows the connected sample geometry.

has not been widely exploited to actively assist in parameter extraction.

In this paper, we demonstrate the successful extraction of multiple material parameters by a data analysis method that is based on an FEA model of the test structure. By incorporating a 3-D model of the test structure, we are able to handle varying test structure geometries. Our model-based approach also detects test structure geometries that will result in an inherently large measurement uncertainty. Using a multidimensional parameter optimization scheme, we are able to simultaneously extract several parameters from the test data. These can be the thermal conductivities of several materials in a stack, or the temperature dependency of the properties of a single film, or some combination of these.

Section II describes the microelectrothermal test structure, the experimental procedure, and the experimental results, which demonstrate our approach using aluminum samples on silicon nitride membranes. Section III presents the parameter estimation. Though thermal properties of silicon nitride films have been reported in the literature [8], here, thermal conductivity of neither the aluminum nor the silicon nitride is assumed to be known *a priori*. Parameters are extracted using nonlinear least squares optimization by the Nelder–Mead simplex algorithm. The resulting estimates are significantly lower than the bulk values, which is consistent with alternative measurement methods and trends observed elsewhere in the literature. In Section IV, we describe details of the errors and sensitivity of the method, and how geometries that lead to inherently inaccurate measurements may be identified prior to device fabrication. Finally, Section V summarizes our results and discusses future research directions.

II. Experimental Procedure and Measurement Results

Fig. 1 is a schematic of the test device cross section. Fig. 2 shows plan-view optical micrographs with two different sample geometries. Silicon nitride layers, 180 nm thick, are deposited on both sides of a silicon wafer using plasma-enhanced chemical vapor deposition (PECVD) at 350 °C. All patterning is carried out using I-line contact lithography and standard commercial resists. The back side SiN_x layer is patterned, and a selective KOH wet etch is used to produce the 360 × 160 μm suspended SiN_x window structure. These steps are followed by depositing the 280 μm× 80 μm× 140 nm thick Al sample via electron-beam evaporation, completing the device encapsulation with a 210-nm-thick silicon nitride capping layer and depositing the 30-nm-thick 5-μm-wide Ni heater and detector. Both metallization steps are liftoff processes.

One serpentine structure was designated as a heater/sensor, the other was used purely as a sensor. For convenience, we will subsequently refer to the heater/sensor structure as the heater, with the understanding that it is also used to monitor temperature. The electrical resistance of the heater was determined while applying a known dc current. The heater and sensor resistances were measured using a calibrated ohmmeter (Keithley 2400). Heater and sensor resistances were calibrated by immersion into a water bath of a known temperature, and the resistance–temperature slope was established by a least squares linear fit to the data, i.e., $\Delta T = \alpha_{L/S} \Delta R_e$, for the heater and sensor. The coefficient $\alpha_{L/S}$ is the *temperature coefficient of resistance* (TCR), and it describes the sensitivity of the RTD.

The electrical resistance of both the heater and the sensor were measured at ambient temperature and atmospheric pressure, and then for ten different applied heater voltages, again, at atmospheric pressure. The temperatures of the heater and sensor were determined using $T_h = T_{\text{ambient}} + \alpha_{L/S} \Delta R_{e,h}$ and $T_s = T_{\text{ambient}} + \alpha_{L/S} \Delta R_{s,h}$, respectively. Fig. 3 shows the applied voltages and the resulting T_h and T_s. Data for the device with the connected (disconnected) Al sample are shown in Fig. 3(a) and (b), corresponding to the micrograph in Fig. 2(a) and (b). The curves in Fig. 3 are from the FEA model, incorporating optimal parameter estimates, as described in Section III. A number of factors make these results difficult to interpret using a simple analytical form. For one, the temperature over both the heater and sensor varies significantly. In addition, the heat flow is through all sides of the sample and membrane to the frame. Finally, the temperature significantly varies over the supporting membrane, whose thermal properties are temperature dependent. Although a closed-form model is unavailable, we find that an FEA model is capable of extracting meaningful thermal properties of the materials in the device.

III. Model-Based Parameter Estimation

Three-dimensional conductive heat flow in the test structure stack is modeled using the ANSYS FEA package [23]. Fig. 4(a) shows a typical element mesh. To construct an accurate but computationally efficient model, it is necessary to identify which mechanisms govern heat flow. Generally, these may include conduction, convection, and radiation. Estimates of the relative magnitudes of these components are given in Table I, which shows that conduction is dominant by two orders of magnitude. To verify that convection was in fact negligible, ANSYS simulations were done, including convective heat loss through the top and bottom of the device using a heat transfer coefficient of 10 $W/m^2 \cdot K$. The change in temperature at the highest power level was less than 0.05% for both the heater and the sensor. Based on these results, we consider only conduction in our model.

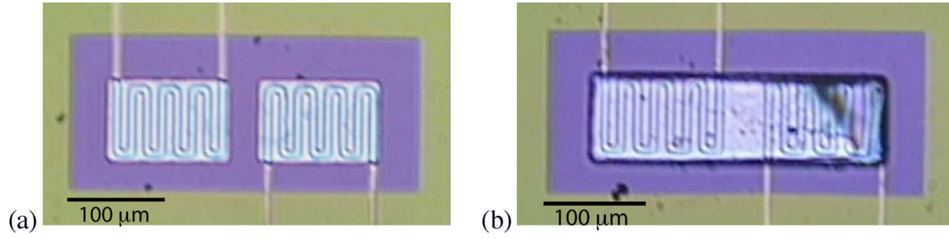

Fig. 2. Top-down optical micrographs of two test devices. The silicon substrate frame is visible around the borders of the photographs; the suspended nitride membrane forms the central region in both pictures. The nickel serpentine structures are identical in the two devices, whereas the aluminum samples have (a) disconnected and (b) connected geometries. Electrical connections are made to 200 μm square Ni bond pads using a probe station. The bond pads are located at 350 μm from the sample.

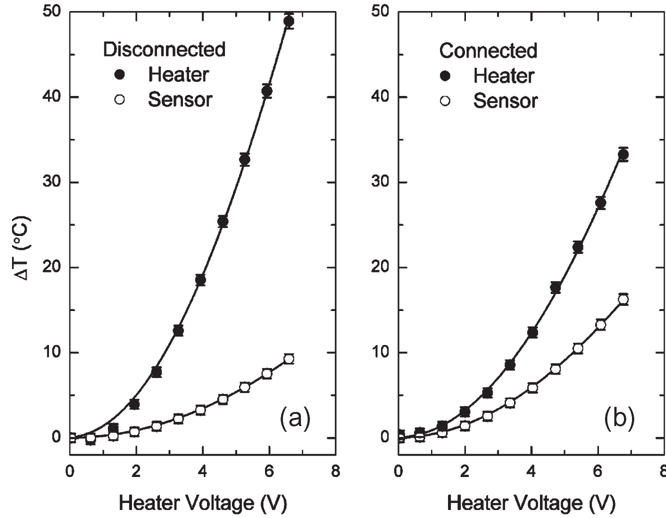

Fig. 3. Heater and sensor temperature rises above ambient at various heater voltages. (a) Disconnected Al sample. (b) Connected Al sample. Solid curves are from the FEA model, incorporating optimal parameter estimates, which were obtained as described in Section III.

Treating the thick silicon frame as a heat sink, the edge of the nitride membrane is held at the ambient temperature. All other surfaces are insulated, following the assumption of negligible convection and radiation. A volume heat generation load is applied in the elements that represent the serpentine heater. The total thermal power generated in the heater is determined using

$$P_h = I^2 R_{e,h} \tag{1}$$

where I is the current applied to the heater, and $R_{e,h}$ is the electrical resistance of the serpentine heater, which is computed based on resistivity measurements using the transmission line method (TLM) to account for contact resistance [30] and verified against literature values for a 30-nm-thick nickel [25]. Both give a value of $9 \times 10^{-8}\ \Omega \cdot \mathrm{m}$. We have checked this thermal simulation against more comprehensive electrothermal simulations in which current is applied directly to the serpentine heater in the ANSYS model. The results were in good agreement, and thus, we subsequently used the purely thermal model for computational efficiency. The total input power is uniformly distributed over the heater volume elements. The two simulation outputs were the volume-averaged temperature in the heater elements $\hat{T}_h$ and the volume-averaged temperature in the sensor elements $\hat{T}_s$. The simulation was implemented as a macro in the ANSYS parametric design language (APDL) [23] to allow material properties such as thermal conductivity to be systematically varied.

A weighted root-sum-square error criterion was adopted to quantify the accuracy of the model. A series of input power levels $P_{hi}, i = 1, \ldots, N$, was measured and simulated for both devices. The measured heater and sensor temperatures are denoted T_{hi} and T_{si}, respectively. Simulated heater and sensor temperatures are denoted $\hat{T}_{hi}$ and $\hat{T}_{si}$, respectively. Then, the error associated with a particular set of simulations is given by

$$J^2 = \sum_{i=1}^{N} W(T_{hi}) \left(T_{hi} - \hat{T}_{hi}\right)^2 + \sum_{i=1}^{N} W(T_{si}) \left(T_{si} - \hat{T}_{si}\right)^2 \tag{2}$$

where $N = 10$ is the number of measurements. The weighting factor is given by $W(T) = 1/\sigma(T)$, where $\sigma(T) = \sqrt{\sigma_{\mathrm{abs}}^2 + \sigma_{\mathrm{rel}}^2(T)}$, σ_{abs} is an absolute error due to uncertainty in the ambient temperature, and $\sigma_{\mathrm{rel}}(T)$ is a relative error term due to the accuracy of the temperature sensor measurements. Measured ambient temperature variations over the course of an experiment give $\sigma_{\mathrm{abs}} = 0.5\ ^\circ\mathrm{C}$. The relative term is found from $\sigma_{\mathrm{rel}}(T) = \mu \Delta T$, where μ is the relative error in the temperature measurement. It is more convenient to estimate this from the applied power by first estimating the thermal resistance R_t of the test structure by fitting a straight line to the ΔT versus P plots. As seen in Fig. 5, this relationship is well modeled by a linear fit. Note that the resistances of the heater and sensor—$R_{t,h}$ and $R_{t,s}$, respectively—are different. Then, $\sigma_{\mathrm{rel}}(T_{hi}) = \mu R_{t,h} P_i$ and $\sigma_{\mathrm{rel}}(T_{si}) = \mu R_{t,s} P_i$. The relative error μ was taken as 0.07% [26].

Parameters were extracted from the model by minimization of the error function given by (2). An APDL macro was written, implementing the Nelder–Mead downhill simplex method [27]. This is a robust minimization algorithm that does not require analytical expressions for the derivatives of the cost function. In bulk samples, it is known that the thermal conductivity of silicon nitride has a significant temperature dependence, whereas that of aluminum has only a small temperature dependence over the temperature range of interest [8]. Therefore, the three parameters estimated were k_{Al}, $k_{\mathrm{SiN},0}$, and β_{SiN}, where $k_{\mathrm{SiN}} = k_{\mathrm{SiN},0} + \beta_{\mathrm{SiN}} \Delta T$, $k_{\mathrm{SiN},0}$ is the value of thermal conductivity at the ambient temperature of $T_0 = 27\ ^\circ\mathrm{C}$, β_{SiN} is the slope of silicon nitride thermal conductivity versus temperature, and $\Delta T = T - T_0$. The algorithm was considered to have converged when the relative change in the error was less than 0.01%. Typical runs required 50 function evaluations,

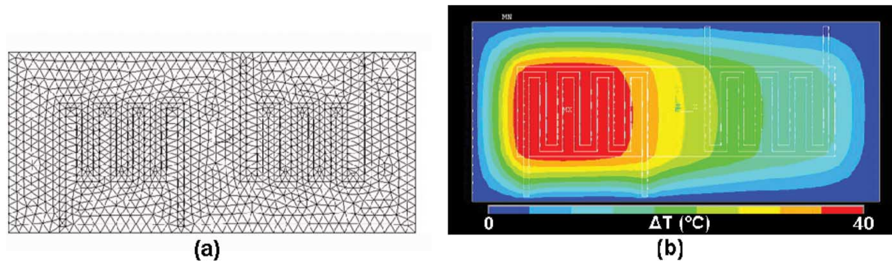

Fig. 4. (a) Top-down view of element mesh for the test device simulation. (b) Simulated temperature distribution for the connected sample using optimal thermal conductivity estimates at an input voltage level of 6.768 V.

TABLE I
ESTIMATED MAGNITUDE OF HEAT FLOW DUE TO CONDUCTION, CONVECTION, AND RADIATION

Mechanism	Governing Equation	Heat Flow Q	Value (W)
Conduction	Fourier's Law	$kA_s(T_s - T_0)/l$	5.3×10^{-3}
Convection	Newton's Law of Cooling	$hA_t(T_s - T_0)$	2.2×10^{-5}
Radiation	Stephan-Boltzmann Law	$\varepsilon\sigma A_t T_s^4$	2.7×10^{-5}

Parameters: T_s: sample temperature (highest measured temperature ~ 77°C); T_0: ambient temperature (27°C); L: sample length (280μm); W: sample width (80μm); t: membrane thickness (0.39μm); l: distance from sample to frame (40 μm); A_s: cross-sectional membrane area ~ $2(W+L)t$ (2.8×10^{-10}m^2); A_t: exposed planar sample area ~ $2WL$ (4.4×10^{-8} m^2); k: thermal conductivity (15-30 W/mK is the bulk value for silicon nitride [24]); h: convective heat transfer coefficient (typically ≤ 10 W/m^{2}K for free convection at atmospheric pressure, set here to 10 as the worst case [24]); ε: emissivity (usually less than 0.8, set here to 1 as the worst case [24]); σ: Stefan-Boltzmann constant (5.67×10^{-8} W/m^{2}K^4 [24]).

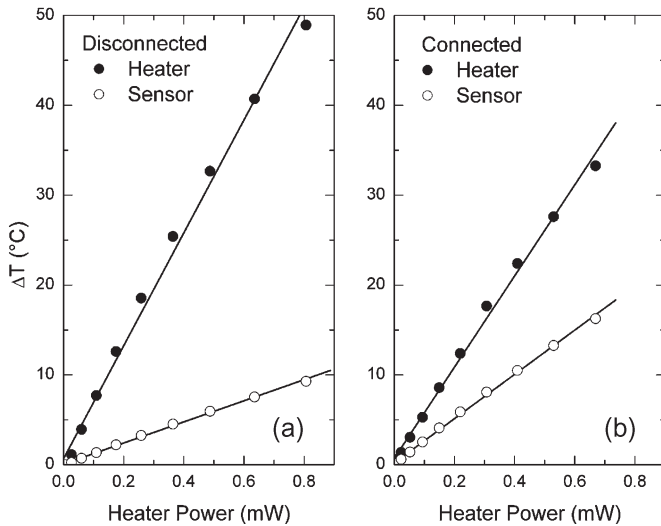

Fig. 5. Temperature rise from ambient versus power data, showing a linear relationship with the goodness-of-fit $R^2 > 0.99$ in all cases. This fit is used only to select weights for the cost function (2) and to estimate error bars.

each entailing ten separate ANSYS simulations (one for each power level).

Results for the three material properties are given in Table I for the connected and disconnected geometries. Fig. 3 compares the temperatures that were predicted from the ANSYS simulation using the optimal estimates to the measured values. Fig. 4(b) shows the simulated temperature distribution for one power level.

As can be seen in Table II, the connected sample best estimates parameters k_{Al} and $k_{\mathrm{SiN},0}$. The disconnected sample should only be used to estimate $k_{\mathrm{SiN},0}$. The size of the relative uncertainties in the results is calculated using numerically computed sensitivities, as described in Section IV. These calculations elucidate how the FEA model can be used to match test devices and data sets with the accurate measurement of specified properties.

The value of 94 W/mK that we obtain for k_{Al} using the connected geometry is much lower than the bulk value of ~237 W/mK [28]. Although we are aware of no other studies on thermal conductivity of aluminum films in this thickness range, the reduction from the bulk value is consistent with previous studies in other materials. For example, studies of the thermal conductivity of copper give the bulk value of ~402 W/mK (room temperature) for film thicknesses that are greater than 400 nm [29]. Below 400 nm, the thermal conductivity is lower than the bulk value. At a thickness of ~140 nm, the Cu thermal conductivity decreases to ~220 W/mK [29] or ~55% of the bulk value. In this paper, we find that an Al film of 140 nm has a thermal conductivity that is ~41% of the bulk value for Al. The reduced thermal conductivity with decreasing film thickness of polycrystalline materials is generally attributed to increased carrier scattering at grain boundaries [5]. Thus, for a given material, the thermal conductivity may even depend on the deposition method [29] due to variations in the formation of polycrystals and their boundaries. Although we do not expect the behaviors of two different metals to exhibit identical dependences with thickness, it is satisfying that our reduced thermal conductivity is qualitatively consistent with the trend that is established for Cu. The Wiedemann–Franz law may be used to provide a quantitative check on the value of k_{Al}. The Wiedemann–Franz law [29] states that at absolute temperature T, the ratio of thermal conductivity k to electrical conductivity σ is given by $k/\sigma = LT$, where L is the *Lorentz number*, which, for aluminum, is 2.09×10^{-8} WΩ/K^2 [29]. Applying the TLM [30] to an aluminum film of the same thickness and deposited under same conditions as the original sample we measure an electrical resistivity of $6.44 \times 10^{-8}\ \Omega \cdot \mathrm{m}$. The Wiedemann–Franz Law then predicts a thermal conductivity of 97.4 W/mK, which is within experimental uncertainty of our

TABLE II
THERMAL CONDUCTIVITY PARAMETER ESTIMATION FOR CONNECTED AND DISCONNECTED GEOMETRIES

	$k_{\mathrm{SiN},0}$ (W/mK)	β_{SiN} (W/mK^2)	k_{Al} (W/mK)
Connected sample	2.07 ± 0.15	(0.006 ± 0.014)	93.9 ± 5.5
Disconnected sample	2.02 ± 0.18	(0.007 ± 0.012)	(77.3 ± 202)

All quantities are given for a nominal temperature of 27 ºC. Values in parentheses have large associated relative uncertainties and are included only for comparison purposes. Computation of errors and sensitivities is discussed in Section III.

value obtained solely from thermal analysis. We remark that for thin metal films the Wiedemann–Franz law may often be used obtain thermal conductivity. The direct measurement method presented here, however, is also applicable to materials such as semiconductors, for which the Wiedemann–Franz law does not hold. The primary goal of the present paper is to demonstrate the use of FEA models for parameter estimation. Aluminum is well suited to this purpose because the Wiedemann–Franz law is expected to hold, and electrical resistivity measurements may be used as a check on the thermal conductivity results.

The results for the thermal conductivity of silicon nitride are also significantly lower than reported bulk values. We obtained values of thermal conductivity for ambient temperature SiN_x of 2.07 ± 0.15 and 2.02 ± 0.18 W/mK for the connected and disconnected devices, respectively. These are in good agreement with each other, and with reported values of 2.23 ± 0.12 W/mK for PECVD nitride of comparable thickness and deposition conditions [8]. The relative error associated with our estimate is under 10%. Our β_{SiN} values from the connected and disconnected devices are also consistent and within the experimental error value of $0.002{-}0.003$ W/mK^2, which is estimated from the data in [8]. However, the relative measurement errors are large, a result that is attributed to the smallness of this quantity and the overall narrow temperature range produced in our experiments, with measured average heater temperatures ranging from ambient (i.e., 27 °C) to a high of 77 °C. A better estimate could be obtained through a series of measurements at different ambient temperatures, as in [8], and this is clearly desirable for situations where the temperature dependence is critical.

IV. ERRORS AND SENSITIVITY

The errors reported in Table II were obtained by numerical sensitivity analysis. Any of the thermal conductivity parameters can be considered as a function of the measured temperatures, i.e., $p = f_p(T_1, \ldots, T_N)$, where p is k_{Al}, $k_{\mathrm{SiN},0}$, or β_{SiN}. The uncertainty of the parameter may be written in terms of the uncertainties in the temperature measurements as

$$\sigma_{k_x}^2 = \sum_{i=1}^{N} \left(\frac{\partial p}{\partial T_i} \right)^2 \sigma_{T_i}^2. \tag{3}$$

Because we do not have analytical expressions for the partial derivatives in (3), we numerically approximate them by $\partial p/\partial T_i \approx \Delta p/\Delta T_i$. Here, one measured temperature is changed by a small $T_i' = T_i + \Delta T_i$ (typically, $\Delta T \sim 0.25$ °C), and a new set of parameters p' is obtained by reminimizing the cost (2). Then, $\Delta p = p' - p$. This process is separately repeated for each measured temperature. The minimization quickly converges since the small change in measured temperature does not usually cause a large change in the optimal parameter values.

TABLE III
MAXIMUM PARAMETER SENSITIVITIES FOR CONNECTED AND DISCONNECTED GEOMETRY USING MEASURED DATA AND OPTIMAL PARAMETER VALUES

	$S_{k\mathrm{SiN,\,max}}$	$S_{\beta\mathrm{SiN,\,max}}$	$S_{k\mathrm{Al,max}}$
Connected	0.51	(22)	0.95
Disconnected	1.1	(49)	(54)

From the sensitivity calculations the estimates in parentheses—of k_{A1} for the disconnected geometry and of the temperature dependence of β_{SiN} for both geometries—are seen to have inherently large relative uncertainties. Test devices should only be used for measurement of a particular property if the associated sensitivity is of order unity or lower.

The numerical partial derivatives used in (3) may also be used to compute the sensitivity of the extracted thermal conductivity values to the measured temperatures. The sensitivity of parameter p to measurement T_j is defined by

$$S_{p,j} \equiv \frac{\delta p}{p} \Big/ \frac{\delta T_j}{T_j} = \frac{T_j}{p} \frac{\partial p}{\partial T_j} \tag{4}$$

where δT_j represents a small variation in the jth temperature (independent parameter), and δp is the resulting change in the dependent parameter p. As can be seen from comparing (4) with the error expression (3), the sensitivity describes the amplification of relative errors from a particular measurement to the estimated parameter value. Therefore, large sensitivities $(S_{p,j} \gg 1)$ will correspond to an inherently inaccurate measurement. Table III gives the maximum sensitivities of the estimated parameters to the temperature measurements for the connected and disconnected geometries. The high sensitivities of β_{SiN} from the connected and disconnected devices, and of k_{Al} in the disconnected device, are evident and correspond to the large uncertainties seen in the respective values in Table II. The high sensitivity of k_{Al} in the disconnected device may be physically understood. In steady state, the two pieces of the aluminum sample each reach a nearly uniform temperature, and heat transfer is limited by flow through the nitride membrane. Thus, the relationship between the heater and sensor temperatures is mainly governed by the properties of the nitride. In contrast, in the connected geometry, the heat transfer between the heater and the sensor is primarily through the aluminum sample, and therefore, the temperature difference is strongly influenced by the properties of the aluminum film.

The reason for the high sensitivities of β_{SiN} may be seen in Fig. 4(b). The temperature dependence of the nitride properties must be inferred using the distribution of temperatures in the nitride membrane. However, as seen in the figure, a relatively small portion of the membrane is actually at an elevated temperature. For the devices considered, estimation of properties at the ambient temperature is therefore more accurate than at

TABLE IV
MAXIMUM PARAMETER SENSITIVITIES FOR CONNECTED AND DISCONNECTED GEOMETRY USING SYNTHETIC DATA AND PARAMETER VALUES

	$S_{k\mathrm{SiN, max}}$	$S_{\beta\mathrm{SiN, max}}$	$S_{k\mathrm{Al,max}}$
Connected	0.74	(80)	0.76
Disconnected	0.48	(33)	(4.0)

The pattern of parameter estimates with inherently large relative uncertainties (in parentheses) is seen to be the same as in Table II.

higher temperatures. Addressing this, if desired, would require a different device design or additional measurements at varying ambient conditions.

In the analysis above, the sensitivities are computed at the final parameter values, but more generally, they can be numerically explored prior to device fabrication using reasonable values. This analysis may be used to reduce the likelihood of unproductive experiments. This is demonstrated in Table IV, which shows the sensitivities that were obtained from the ANSYS model using bulk values from the literature [28], [29]. Although there are differences, due to the change in patterns of heat flow, the qualitative patterns that indicate inherently large uncertainties are the same. An interesting observation is that the sensitivity of the k_{Al} measurement using bulk values, although still large, is much smaller than the corresponding values that were obtained using the thin-film conductivities. This is because the bulk thermal conductivities of both the aluminum and the nitride are larger than the thin-film values, but not by the same proportion. In fact, the nitride conductivity is ten times higher, whereas the aluminum conductivity is less than three times larger. This means that the bulk values of aluminum and nitride conductivities are closer, so the sample temperatures are less uniform, and the resulting increase in heat flow is associated with a larger influence on the sensor temperatures. As can be seen from this example, a sensitivity analysis using approximate parameter values can provide useful guidance, but this must be used with care.

V. SUMMARY

We have demonstrated a new experimental framework for an accurate measurement of the lateral thermal conductivities of thin films. A microelectrothermal test structure design is integrated with model-based data analysis. For nanoscale layer thickness, parasitic heat flow through the support structure makes simple quantitative analysis of the experiments impractical. We find that it is invaluable to carry out FEA simulations in parallel with the experiments in order to extract quantitative properties of the film. The model is also useful for predicting which material properties may be accurately extracted and for validating experiment designs prior to fabrication. This may translate into significant savings in time and resources compared with a pure trial-and-error approach. Microfabricated sensors and samples were used to qualify the approach on 140-nm-thick Al layers that are supported by a 180-nm-thick silicon nitride membrane. Agreement between the data and the FEA model is excellent (Fig. 3). We obtain thermal conductivities of the Al and SiN_x thin films that are considerably lower than those of the bulk values. The SiN_x results compare well with previously published work on films that have comparable thicknesses [8]. For Al, our value is in agreement with trends described in previous reports, as well as with the result obtained by using electrical resistivity measurement and applying the Wiedemann–Franz law [8], [13], [19], [21], [22], [29].

REFERENCES

[1] D. G. Cahill, H. E. Fischer, T. Klitsner, E. T. Swartz, and R. O. Pohl, "Thermal conductivity of thin films: Measurement and understanding," *J. Vac. Sci. Technol. A, Vac. Surf. Films*, vol. 7, no. 3, pp. 1259–1266, May 1989.

[2] S. M. Lee and D. G. Cahill, "Heat transport in thin dielectric films," *J. Appl. Phys.*, vol. 81, no. 6, pp. 2590–2595, Mar. 1997.

[3] K. E. Goodson, M. I. Flik, L. T. Su, and D. A. Antoniadis, "Annealing-temperature dependence of the thermal conductivity of LPCVD silicon-dioxide layers," *IEEE Electron Device Lett.*, vol. 14, no. 10, pp. 490–492, Oct. 1993.

[4] I. Ahmad, V. Kasisomayajula, D. Y. Song, L. Tian, J. M. Berg, and M. Holtz, "Self-heating in a GaN based heterostructure field effect transistor: Ultraviolet and visible Raman measurements and simulations," *J. Appl. Phys.*, vol. 100, no. 11, pp. 113 718-1–113 718-7, Dec. 2006.

[5] D. G. Cahill, W. K. Ford, K. E. Goodson, G. D. Mahan, A. Majumdar, H. J. Maris, R. Merlin, and S. R. Phillpot, "Nanoscale thermal transport," *J. Appl. Phys.*, vol. 93, no. 2, pp. 793–818, Jan. 2003.

[6] D. L. DeVoe, "Thermal issues in MEMS and microscale systems," *IEEE Trans. Compon. Packag. Technol.*, vol. 25, no. 4, pp. 576–583, Dec. 2003.

[7] X. Liu, M. H. Hu, C. G. Caneau, R. Bhat, and C. Zah, "Thermal management strategies for high power semiconductor pump lasers," *IEEE Trans. Compon. Packag. Technol.*, vol. 29, no. 2, pp. 493–500, Jun. 2006.

[8] M. von Arx, O. Paul, and H. Baltes, "Process dependent thin film thermal conductivities for thermal CMOS MEMS," *J. Microelectromech. Syst.*, vol. 9, no. 1, pp. 136–145, Mar. 2000.

[9] A. D. McConnell and K. E. Goodson, "Thermal conduction in silicon micro- and nanostructures," *Annu. Rev. Heat Transf.*, vol. 14, pp. 129–168, 2005.

[10] Y. C. Tai, C. H. Mastrangelo, and R. S. Muller, "Thermal conductivity of heavily doped low-pressure chemical vapor deposited polycrystalline silicon films," *J. Appl. Phys.*, vol. 63, no. 5, pp. 1442–1447, 1988.

[11] D. G. Cahill, "Thermal conductivity measurement from 30 to 750 K: The 3ω method," *Rev. Sci. Instrum.*, vol. 61, no. 2, pp. 802–808, 1990.

[12] E. Jansen and E. Obermeier, "Thermal conductivity measurements on thin films based on micromechanical devices," *J. Micromech. Microeng.*, vol. 6, no. 1, pp. 118–121, Mar. 1996.

[13] L. La Spina, N. Nenadovic, A. W. van Herwaarden, H. Schellevis, W. H. A. Wien, and L. K. Nanver, "MEMS test structure for measuring thermal conductivity of thin films," in *Proc. IEEE Int. Conf. Microelectron. Test Struct.*, Mar. 6–9, 2006, pp. 137–142.

[14] C. Dames and G. Chen, "1ω, 2ω, and 3ω methods for measurements of thermal properties," *Rev. Sci. Instrum.*, vol. 76, p. 124 902, 2005.

[15] C. H. Mastrangelo, Y. C. Tai, and R. S. Muller, "Thermophysical properties of low-residual stress, silicon-rich, LPCVD silicon nitride films," *Sens. Actuators*, vol. A23, pp. 856–860, 1990.

[16] F. Völklein, "Thermal conductivity and diffusivity of a thin film SiO–SiN sandwich system," *Thin Solid Films*, vol. 188, pp. 27–33, 1990.

[17] F. Völklein and H. Baltes, "A microstructure for measurement of thermal conductivity of polysilicon thin films," *J. Microelectromech. Syst.*, vol. 1, no. 4, pp. 193–196, Dec. 1993.

[18] T. Stärz, U. Schmidt, and F. Völklein, "Microsensor for in situ thermal conductivity measurements of thin films," *Sens. Mater.*, vol. 7, pp. 395–403, 1995.

[19] O. Paul and H. Baltes, "Determination of the thermal conductivity of CMOS IC polysilicon," *Sens. Actuators*, vol. A41/42, pp. 161–164, 1994.

[20] A. Rosencwaig, J. Opsal, W. L. Smith, and D. L. Willenborg, "Detection of thermal waves through optical reflectance," *Appl. Phys. Lett.*, vol. 46, no. 11, pp. 1013–1015, 1985.

[21] A. Jacquot, W. L. Liu, G. Chen, J.-P. Fleurial, A. Dauschera, and B. Lenoir, "Improvements of on-membrane method for thin-film thermal conductivity and emissivity measurements," in *Proc. 21st ICT*, 2002, pp. 353–356.

[22] A. Jacquot, B. Lenoir, A. Dauscher, M. Stolzer, and J. Meusel, "Numerical simulation of the 3ω method for measuring the thermal conductivity," *J. Appl. Phys.*, vol. 91, no. 7, pp. 4733–4738, Apr. 2002.

[23] *ANSYS User's Guide, Release 10.0A1*, ANSYS, Inc., Canonsburg, PA, 2006.

[24] F. P. Incropera and D. P. DeWitt, *Fundamentals of Heat and Mass Transfer*, 5th ed. New York: Wiley, 2002.
[25] C. K. Ghosh and A. K. Pal, “Electrical resistivity and galvano metric properties of evaporated nickel films,” *J. Appl. Phys.*, vol. 51, Apr. 1980.
[26] *Model 2400 Series: SourceMeter, Quick Results Guide*, Keithley Instruments, Inc., Cleveland, OH, 2000. Document 2400S-903-01 Rev. C.
[27] W. H. Press, S. A. Teukolsky, W. T. Vetterling, and B. P. Flannery, *Numerical Recipes: The Art of Scientific Computing*. Cambridge, U.K.: Cambridge Univ. Press, 1986.
[28] D. R. Lide, *CRC Handbook of Chemistry and Physics*, 86th ed. New York: Taylor & Francis, 2005.
[29] T. M. Tritt, *Thermal Conductivity: Theory, Properties, and Applications*. New York: Plenum, 2004.
[30] H. H. Berger, “Contact resistance and contact resistivity,” *J. Electrochem. Soc.*, vol. 119, no. 4, pp. 507–514, 1972.

Nenad Stojanovic received the B.S. degree from Wayland Baptist University, Plainview, TX, in 2005. He is currently working toward the M.S. degree at the Department of Physics, Texas Tech University, Lubbock.

He is also currently a Research Assistant in the Nano Tech Center, Texas Tech University, working on thermal conductivity of nanoscale films and nanowires. His research includes microfabrication of thermal sensors, nanofabrication of sample films and nanowires, and finite-element simulation of devices for guiding fabrication and interpreting data.

Jongsin Yun received the M.S. and Ph.D. degrees in electrical engineering from Texas Tech University, Lubbock, in 2000 and 2005, respectively. His Ph.D. research was metal contact formation on wide-bandgap semiconductor materials (AlGaN), which are used in deep-UV optical devices.

He is currently a Senior Engineer with the System LSI Technology Development Group, Samsung Semiconductor, Seoul, Korea, conducting research and development in SRAM and related areas. He is involved in developing 65-nm-node and 45-nm-node SRAMs in SOC for low-power application.

Erika B. K. Washington received the B.S. degree in mechanical engineering from the University of Colorado, Boulder, in 1992 and the M.S. degree in mechanical engineering from Texas Tech University, Lubbock, in 2005. She is currently working toward the Ph.D. degree in mechanical engineering in the Department of Mechanical Engineering, University of Alberta, Edmonton, AB, Canada.

She was with the manufacturing industry as a Production and Project Manager. Her current research interest is the behavior of materials at the microscale or nanoscale, in particular segmented flow in microfluidics.

Jordan M. Berg (M’91–SM’00) received the B.S.E. and M.S.E. degrees in mechanical and aerospace engineering from Princeton University, Princeton, NJ, in 1981 and 1984, respectively, and the Ph.D. degree in mechanical engineering and mechanics and the M.S. degree in mathematics and computer science from Drexel University, Philadelphia, PA, in 1992.

He has held postdoctoral appointments at U.S. Air Force Wright Laboratory, Dayton, OH, and the Institute for Mathematics and Its Applications, Minneapolis, MN. Since 1996, he has been with Texas Tech University, Lubbock, where he is currently an Associate Professor of mechanical engineering and an Associate Director of the Nano Tech Center. His research interests include control theory, modeling, simulation, and design of nanosensors and microsensors, modeling, simulation, and design of microfluidic systems, modeling, simulation, design, fabrication, and control of electrostatic NEMS and MEMS, and engineering education and outreach.

Dr. Berg is a member of the American Society of Mechanical Engineers (ASME) since 2002.

Mark W. Holtz received the B.S. degree in physics from Bradley University, Peoria, IL, in 1980, and the Ph.D. degree in physics from Virginia Polytechnic Institute and State University, Blacksburg, in 1987.

From 1987 to 1989, he was a Postdoctoral Fellow at the Max Planck Institute FKF, Stuttgart, Germany. From 1989 to 1991, he was a Research Associate at Michigan State University, East Lansing. Since 1991, he has been with the faculty of the Department of Physics, Texas Tech University, Lubbock, where he is currently a Professor. He also serves as Co-Director of the Nano Tech Center. He has held visiting positions at Intel Corporation and Texas Instruments, Inc. His research interests include optical properties of semiconductors, plasma processing of nanophotonic structures, self-assembly, and materials physics.

Henryk Temkin (SM’87–F’93) received the B.S. degree in physics from the Universite Libre de Bruxelles, Brussels, Belgium, in 1969, the M.A. degree in physics from Yeshiva University, New York, NY, in 1972, and the Ph.D. degree in physics from Stevens Institute of Technology, Hoboken, NJ, in 1975.

He is a Professor and the Jack Maddox Chair of Electrical Engineering at Texas Tech University, Lubbock. He is currently on leave to serve as Program Manager in the Defense Advanced Research Projects Agency Microsystems Technology Office. During 1992–2005, he taught at Colorado State University, focusing on large-bandgap semiconductors, carrier dynamics in lasers, and integrated optics. Between 1977 and 1992, he was a member of Technical Staff at Bell Laboratories and a Distinguished member of Technical Staff at AT&T Bell Laboratories, Murray Hill, NJ. In this position, he made a number of contributions to the study of optical and electrical properties of semiconductors, physics and technology of semiconductor lasers, development of quantum-well lasers for optical communications, and development of advanced epitaxial growth methods. He is the author of more than 400 technical publications, including one monograph and one edited book.